Influence of Sample Placement on the Dose Uniformity in Plasma Immersion Ion Implantation of Industrial Ball Bearings

Zhaoming Zeng, Xiubo Tian, Dixon Tat-Kun Kwok, *Member, IEEE*, Baoyin Tang, and Paul K. Chu, *Member, IEEE*

***Abstract*— Plasma immersion ion implantation (PIII) is an effective technique to enhance the surface properties of industrial components possessing an irregular shape. However, it is difficult to achieve uniform implantation along the groove surface of a ball bearing. In this work, we focus on the PIII treatment of the arc surface of an industrial ball bearing. Three practical sample placement configurations are investigated: I) direct placement on the sample stage platen, II) placement on a copper extension with the same diameter as the bearing race, III) placement on a copper plate erected on the sample stage by means of a small metal rod. Using theoretical simulation, the implant dose uniformity along the groove surface is determined for the three orientations. Our results reveal that configuration III) yields the largest implant dose along the groove surface and the dose uniformity is worse in configuration I). Hence, in order to improve the lateral dose uniformity along the race surface, the bearing should be elevated from the sample.**

***Index Terms*— Bearings, plasma immersion ion implantation, sheath simulation, uniformity of implantation dose.**

I. Introduction

PLASMA immersion ion implantation (PIII) is a burgeoning technology for surface modification of materials [1]–[4]. Because there is no line-of-sight restriction, it is an excellent technique to treat industrial components possessing an irregular shape such as precision bearings [5]. For an industrial ball bearing, the working surface of both the interior and exterior pieces is not flat and has the shape of an arc. Hence, PIII treatment of a ball bearing is as complicated as other odd-shaped targets such as a hollow cylindrical tube used in an oil pump [6]–[9]. The PIII uniformity is an important factor directly affecting the efficacy of surface modification. Therefore, many theoretical and experimental investigations concerning implant uniformity have been performed on specimens possessing various shapes, such as square bars [10], [11], wedge-shaped objects [12]–[14], corners [15], trenches [13], [16], [17], crosses [18], cylindrical tubes [6]–[9], and small cylindrical samples [19], [20]. However, very little work has hitherto been done on real industrial parts and the effects of the sample placement on the implant dose uniformity. Because most industrial ball bearings are not very thick, they are usually laid horizontally on the sample chuck during PIII. However, its close proximity to the sample stage and the insulating shroud surrounding the high voltage feed-through is expected to affect the local implant doses along the race surface. The sheath expansion about the groove surface of an industrial ball bearing for three sample placement configurations is investigated in this work. The sheath potential, ion density, and ion velocity are derived using the fluid model. The variation of the ion implantation dose as well as ion impact angle along the groove is presented and compared for each placement methods.

Manuscript received March 2, 1999; revised May 6, 1999. This work was supported by Hong Kong Research Grants Council Earmarked Grants 9040332 and 9040344 and City University of Hong Kong Strategic Grant 7000964.

Z. Zeng and X. Tian are with the Department of Physics and Material Science, City University of Hong Kong, Kowloon, Hong Kong, China, and Advanced Welding Production and Technology National Key Laboratory, Harbin Institute of Technology, Harbin, China.

D. T.-K. Kwok, B. Tang, and P. K. Chu are with the Department of Physics and Material Science, City University of Hong Kong, Kowloon, Hong Kong, China (e-mail: paul.chu@cityu.edu.hk).

Publisher Item Identifier S 0093-3813(99)06933-7.

II. Sample Placement Methods and Simulation Model

A common industrial ball bearing (model 315) with an interior diameter of 75 mm shown in Fig. 1 is used in our work. In normal operation, the balls roll on the arc surface and it is the focus of our investigation. Owing to the radial symmetry of the ball bearing and the vertical geometry of most PIII vacuum chambers (i.e. the plasma source on top), horizontal placement of the bearing on the sample stage is most convenient. Three practical sample placements are studied:

I) direct placement on the oil-cooled sample stage platen 140 mm in diameter, with the high voltage feed-through shielded by a ceramic shroud 100 mm in diameter and 200 mm tall as illustrated in Fig. 1(a) [21];

II) placement on a 400 mm long metal extension with the same diameter as the bearing on top of the oil-cooled sample stage [Fig. 1(b)];

III) placement on a 2 mm thick metal plate with the same diameter as the bearing erected from the sample stage by a metal rod 5 mm in diameter and 400 mm long [Fig. 1(c)].

For the second and third placement methods, a glass shroud is used to cover the sample stage to minimize the influence of the oil-cooled sample stage.

A plasma with density n_0 is generated in the vacuum chamber. At time $t = 0$, the target potential is switched from $\phi = 0$ to a negative potential $\phi = \phi_t$. An ion-matrix sheath is subsequently induced, and ions are accelerated by

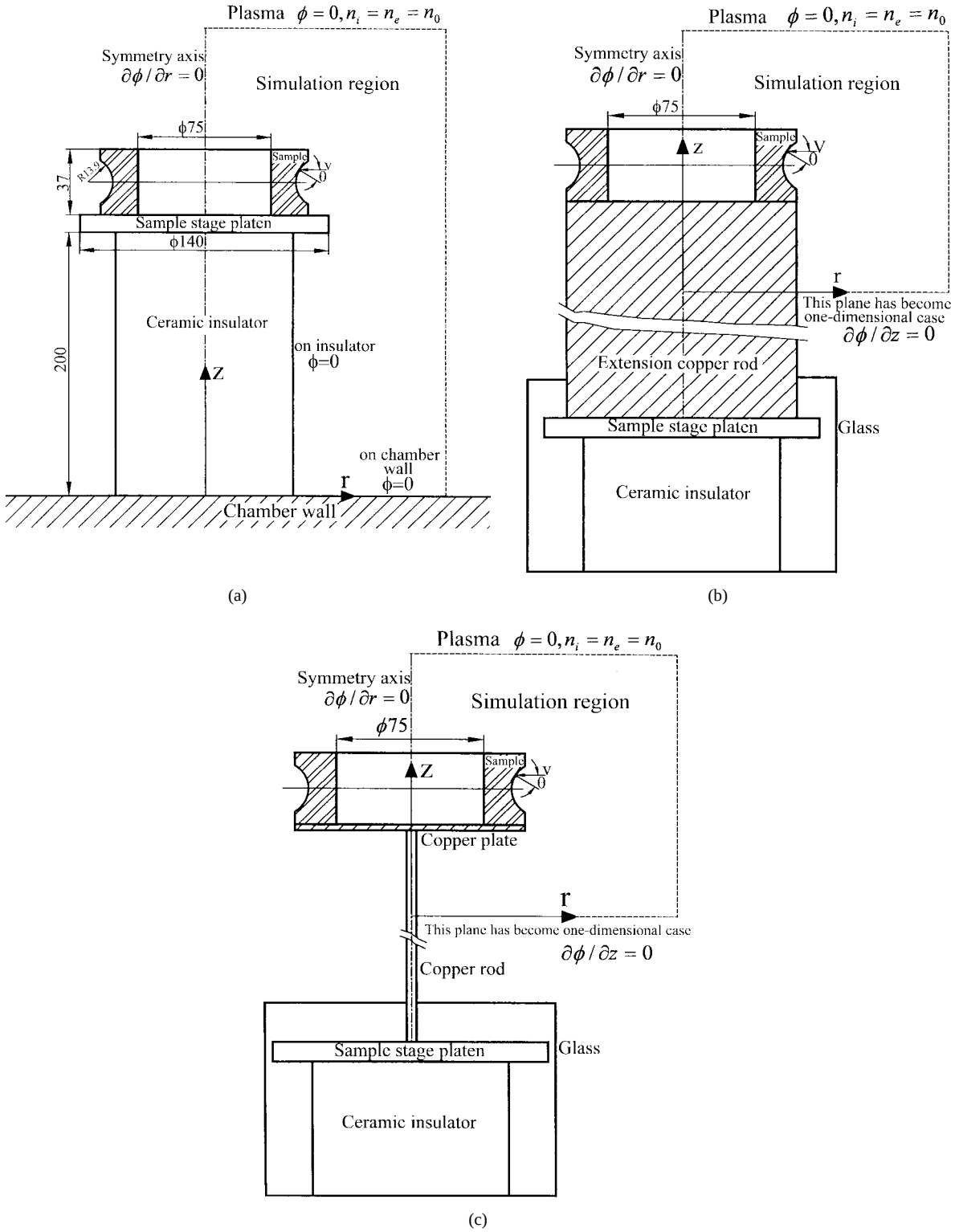

Fig. 1. Schematic presentation of the PIII treatment of the arc surface of an industrial ball bearing. The simulation region is demarcated by the dotted line. The three sample placement configurations are: (a) bearing placed horizontally on the oil-cooled sample stage platen, (b) bearing placed horizontally on a metal extension with the same diameter as the bearing race, and (c) bearing placed horizontally on a metal plate erected vertically from the sample stage by a metal rod.

the electric field and implanted into the target until the applied voltage pulse is over. The evolution of the ion density n_i, ion velocity v_i, and electric potential ϕ can be modeled using cold, collisionless fluid ions, Boltzmann electrons, as well as Poisson's equation [10], [11], [16], [18], [22]. In cylindrical coordinates, the two-dimensional equations of ion continuity and motion, Poisson's equation, and Boltzmann's relation are

$$\frac{\partial n_i}{\partial t} + \frac{1}{r}\frac{\partial}{\partial r}(r n_i v_{ir}) + \frac{\partial}{\partial z}(n_i v_{iz}) = 0 \tag{1}$$

$$\frac{\partial v_{ir}}{\partial t} + v_{ir}\frac{\partial v_{ir}}{\partial r} + v_{iz}\frac{\partial v_{ir}}{\partial z} = -\frac{e}{m}\frac{\partial \phi}{\partial r} \tag{2a}$$

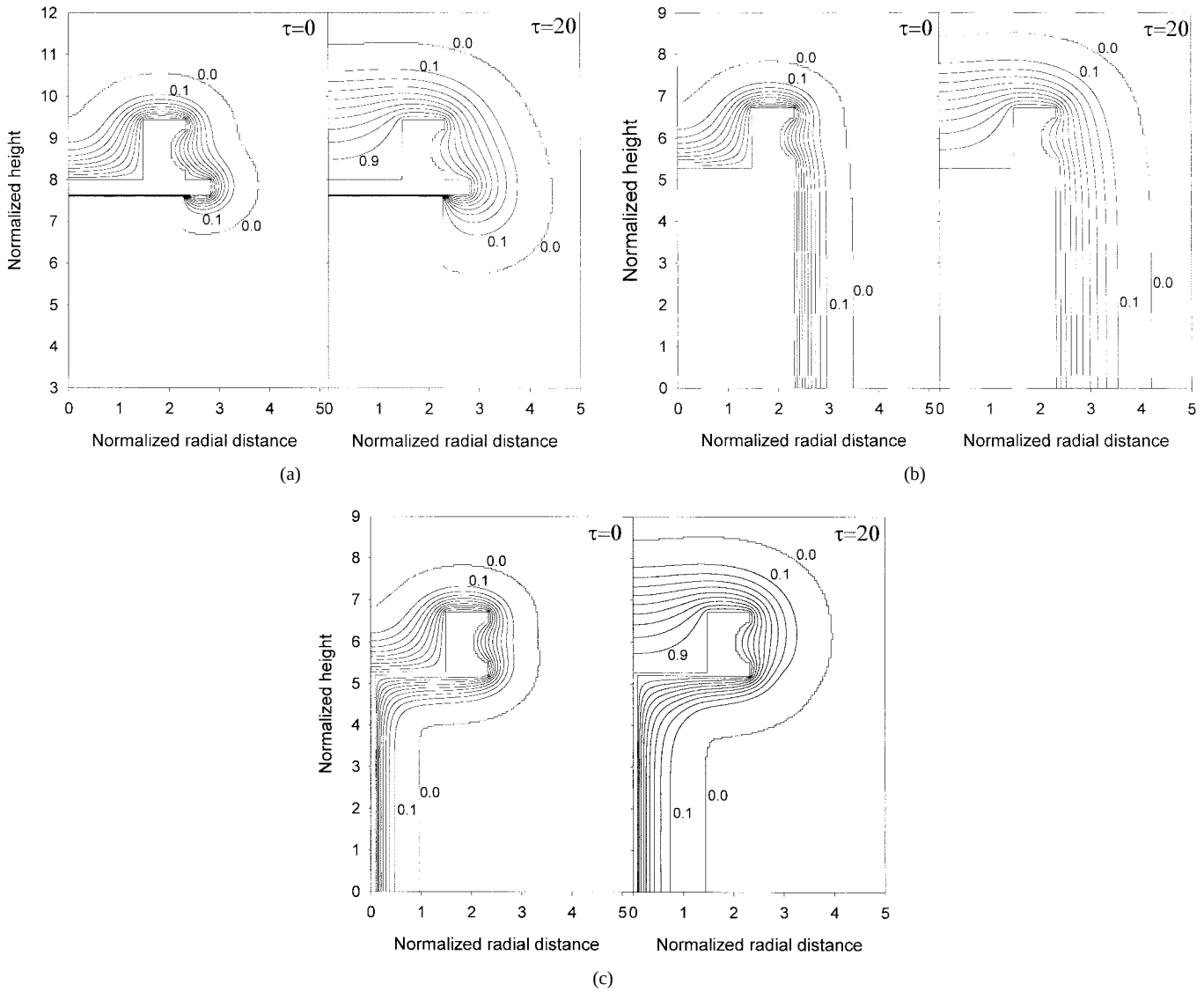

Fig. 2. Evolution of the normalized potential contour lines around the target for the three sample placement configurations on top of (a) the oil-cooled sample stage, (b) the metal extension, and (c) the metal plate shown in Fig. 1.

$$\frac{\partial v_{iz}}{\partial t} + v_{ir}\frac{\partial v_{ir}}{\partial r} + v_{iz}\frac{\partial v_{iz}}{\partial z} = -\frac{e}{m}\frac{\partial \phi}{\partial z} \tag{2b}$$

$$\frac{1}{r}\frac{\partial}{\partial r}\left(r\frac{\partial \phi}{\partial r}\right) + \frac{\partial^2 \phi}{\partial z^2} = -\frac{e}{\varepsilon_0}\left[n_i - n_0 \exp\left(\frac{e\phi}{kT_e}\right)\right] \tag{3}$$

where e is the electron charge (it is assumed that the ions are singly charged) and m is the ion mass. It is more convenient to make (1) to (3) dimensionless by introducing the following variables:

$$R = \frac{x}{s_0}, \quad Z = \frac{z}{s_0}, \quad \psi = \frac{\phi}{\phi_t}, \quad n = \frac{n_i}{n_0},$$
$$u_R = \frac{v_{ir}}{v_{\max}}, \quad u_Z = \frac{v_{iz}}{v_{\max}} \quad \tau = t\omega_{\mathrm{pi}} \tag{4}$$

where $s_0 = \sqrt{-2\varepsilon_0\phi_t/en_0}$ is the planar ion-matrix sheath width, $v_{\max} = \sqrt{-2e\phi_t/m}$ is the velocity that an ion would gain if it fell through a potential drop ϕ_t, and $w_{\mathrm{pi}} = \sqrt{n_0e^2/\varepsilon_0 m}$ is the ion plasma frequency. The equations become

$$\frac{\partial n}{\partial \tau} + \frac{1}{R}\frac{\partial}{\partial R}(Rnu_R) + \frac{\partial}{\partial Z}(nu_Z) = 0 \tag{5}$$

$$\frac{\partial u_R}{\partial \tau} + u_R\frac{\partial u_R}{\partial R} + u_Z\frac{\partial u_R}{\partial Z} = \frac{1}{2}\frac{\partial \psi}{\partial R} \tag{6a}$$

$$\frac{\partial u_Z}{\partial \tau} + u_R\frac{\partial u_Z}{\partial R} + u_Z\frac{\partial u_Z}{\partial Z} = \frac{1}{2}\frac{\partial \psi}{\partial Z} \tag{6b}$$

$$\frac{1}{R}\frac{\partial}{\partial R}\left(R\frac{\partial \psi}{\partial R}\right) + \frac{\partial^2 \psi}{\partial Z^2} = 2\left[n - \exp\left(\frac{e\phi_t}{kT_e}\cdot\psi\right)\right]. \tag{7}$$

The simulation regions are depicted in Fig. 1(a)–(c). The initial conditions are $n = 1$ and $u_R = u_Z = 0$ everywhere. The boundary conditions are $\phi = 1$ on the target, $\phi = 0$ in the plasma, and $\partial\phi/\partial r = 0$ at the central symmetry axis. In Fig. 1(a), the lower boundary is the chamber wall and $\phi = 0$

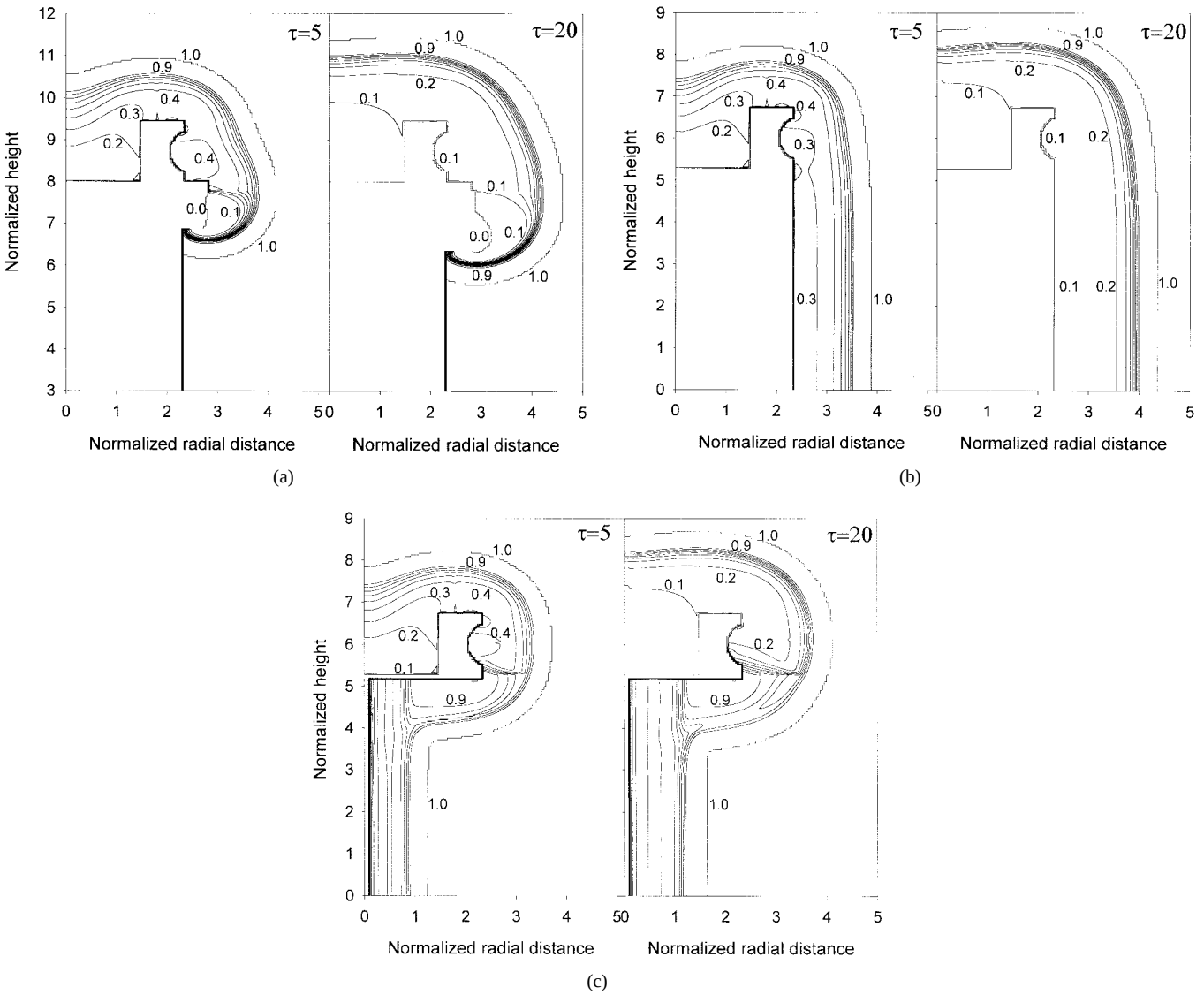

Fig. 3. Evolution of the normalized ion density contour lines around the target for the three sample placement configurations on top of (a) the oil-cooled sample stage, (b) the metal extension, and (c) the metal plate exhibited in Fig. 1.

at this boundary and the ceramic insulator shroud. For the two configurations illustrated in Fig. 1(b) and (c), the metal extension rod is long enough such that $\partial\phi/\partial z = 0$ on the lower boundary of the simulation region as it is far from the bearing sample and can be treated as a one-dimensional case.

The equations are solved by the finite difference method. The simulation parameters are selected to reflect typical experimental conditions: $n_0 = 3.5 \times 10^9$ cm^{-3}, $\phi_t = -20$ kV, $kT_e = 1.5$ eV, and N_2^+ plasma. Hence, $s_0 = 25.1$ mm and $\omega_{\rm pi}^{-1} = 0.0678$ μs. We choose a grid spacing $h = \Delta R = \Delta Z = \frac{1}{25} s_0 \approx 1.0$ mm and a time step of $\Delta\tau = 1/100$. The simulation region is chosen to be $14s_0$ in height and $8s_0$ in the radial direction for configuration (I) shown in Fig. 1(a), and $12s_0$ in height and $8s_0$ in the radial direction for configurations (II) and (III) displayed in Fig. 1(b) and (c), respectively. In configuration (I), the ceramic insulator is relatively long such that the height of the simulation region is chosen to be larger than that in configurations (II) and (III). In this way, the sheath remains inside it throughout the entire simulated time duration. The simulation is conducted to a final step $\tau = 100$ ($t = 6.78$ μs).

III. Results and Discussion

The temporal evolution of the potential contour lines around the target for the three different placement methods is shown in Fig. 2(a)–(c). At $\tau = 0$, the potential distribution of the ion-matrix sheath is shown. The sheath structures around the bearing race differ significantly in the three cases and different implantation characteristics are expected. As the sheath propagates, the conformality of the potential contour to the target surface degrades, and the field lines eventually reach a dome shape in all three situations.

Fig. 3(a)–(c) depict the temporal evolution of the ion density around the target in the three configurations. As expected, the ion density distributions around the bearing groove are quite different for the three placement methods. In configuration (I), due to the influence of the ceramic insulator, there is a zero ion density contour line at $\tau = 5$ under the sample stage platen

indicating that ions are exhausted quickly under the sample stage platen. At $\tau = 5$, the 0.4 ion density contour line near the groove is not symmetrical about the groove center, but rather offset toward the side closer to the sample stage. When $\tau = 20$, only the 0.1 density line exists within the groove. In configuration (II), because the diameter of the extension rod is large, the extension rod also receives a high dose of implanted ions. Therefore, ions in the vicinity of the target are exhausted quickly and there is no ion concentration on the groove surface. In configuration (III), at $\tau = 5$, the 0.4 ion density line near the groove is still symmetrical about the groove center, but ions begin to concentrate on the lower edge. When the sheath expands, this region moves upward. When $\tau = 20$, a large number of ions concentrate within the bearing groove, especially in the lower half, indicating that there are still a large number of ions in the vicinity at this time. Our results thus show that a larger ion dose will be implanted into the groove surface in configuration (III).

Fig. 4(a)–(c) display the distribution and temporal evolution of the ion incident angle relative to the normal along the arc surface (the normal direction is the radial direction). In all three configurations, the ion incident angle near the groove center is smaller than that close to the two edges. Initially, the angle of incidence along the groove surface has a small value and the distribution is almost symmetrical about the center of the race. As the sheath expands, the ions impinge at a more oblique angle, particularly toward the edge. The distribution is also no longer symmetrical. The lower side is bombarded by ions impacting at a smaller angle in all three cases. The spots with almost 0° incident angle (that is, normal incidence) migrate slowly toward the lower side. The worst uniformity with regard to the incident angle is observed for configuration (I) as shown in Fig. 4(a). In this case, the ion impact angle close to the lower edge is much smaller than that near the upper edge. When $\tau = 10$, the incident angle at the upper edge has reached nearly 80°. At a later time, the ions near the upper corner impinge nearly parallel to the surface thereby resulting in more sputtering than implantation. It shows that a lower ion dose will be implanted near the upper edge. In configurations (II) and (III), the incident angle is still larger on the upper side, but the difference is smaller than that observed for case (I), and the ion incident angle near the upper edge is also smaller.

The incident ion dose $D(r,z)$ can be calculated by integrating the ion flux at the target surface

$$D(r,z) = \int_0^{t_p} n_i(t,r,z) \cdot v_{i\perp}(t,r,z)\, dt = \int_0^{t_p} n_i(t,r,z) \sqrt{v_{ir}^2(t,r,z) + v_{iz}^2(t,r,z)} \cos\theta\, dt \tag{8}$$

where t_p is pulse duration and $v_{i\perp}$ is the ion velocity normal to the target surface. The distribution of the ion dose implanted into the arc groove is shown in Fig. 5(a)–(c). The ion dose observed in configuration (III) is 1.5 times larger than that in configurations (I) and (II) except close to the lower edge. It shows that the sample placement illustrated in Fig. 1(c) yields the highest implantation efficiency. In configuration (I), a very small ion dose is implanted into the region near the upper edge [Fig. 5(a)]. After $\tau = 20$, almost no ions are implanted into this area due to the large incident angle near the upper edge. The large incident angle gives rise to higher sputtering loss and less net implantation or a lower retained dose. The ion dose uniformity along the groove surface worsens with increasing implantation time. The uniformity of the ion dose within the groove is better for configurations (II) and (III). In configuration (II), the maximum ion dose is observed near

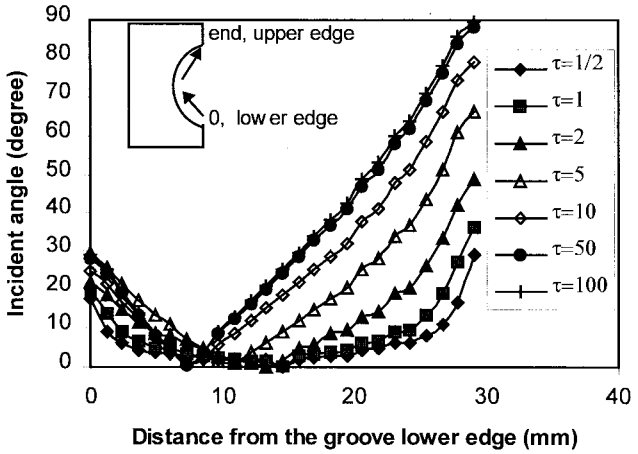

(a)

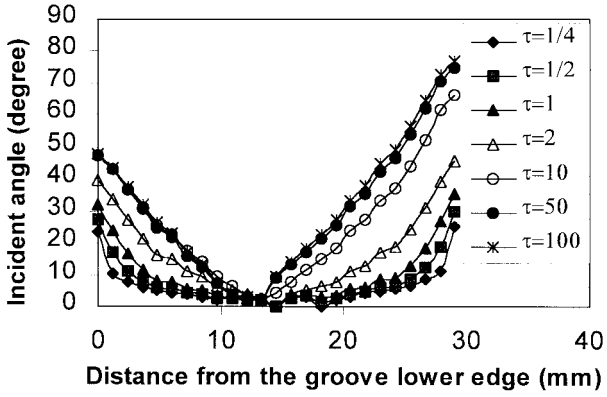

(b)

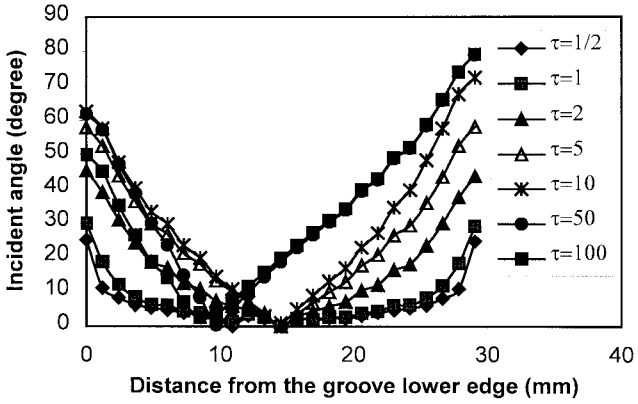

(c)

Fig. 4. Variation of the ion incident angle distributions along the groove surface with time for the three sample placement configurations on top of (a) the oil-cooled sample stage, (b) the metal extension, and (c) the metal plate displayed in Fig. 1.

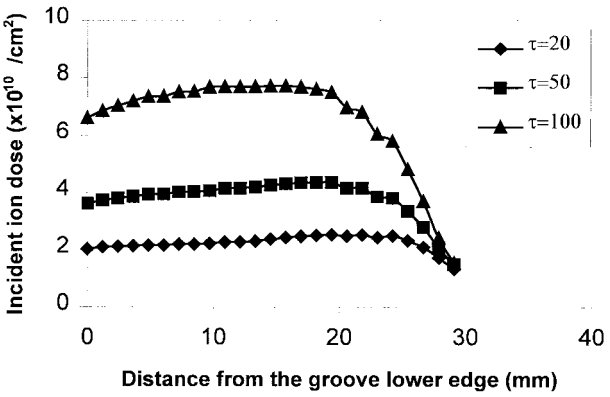

(a)

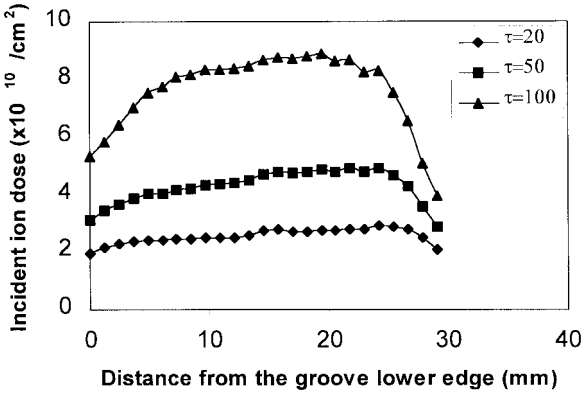

(b)

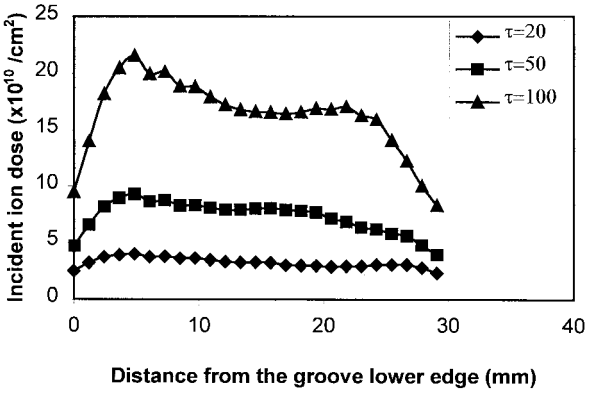

(c)

Fig. 5. Distribution of the ion dose along the bearing groove surface at three different times for the three sample placement configurations on top of (a) the oil-cooled sample stage, (b) the metal extension, and (c) the metal plate depicted in Fig. 1.

the groove center. However, in configuration (III), the largest ion dose is offset toward the lower side. This is caused by the larger ion concentration in the lower half of the groove as aforementioned.

Based on our results, configurations (II) and (III) are better than configuration (I) with regard to ion dose uniformity. In addition, the best implantation efficiency is accomplished in configuration (III). It is thus the most desirable sample placement method. However, because of the metal extension is long but narrow in this configuration, the rate of heat dissipation via the sample stage is compromised. Hence, it is conceivable that if there is a low temperature requirement due to the state of the materials and dimensional tolerances, a lower duty cycle may be necessary to mitigate sample heating. However, if a higher implantation temperature is desirable, for example, to increase the diffusion depth, configuration (III) will be preferred over configurations (I) and (II) as less external heating is required. In comparison, configuration (II) provides better heat dissipation but due to the increased surface area, the total implantation current is inevitably higher. A more potent power modulator may thus be required. Our simulation results indicate that the dose uniformity will be improved by using a shorter pulse $(\tau = 20)$. Hence, pulse lengths of less than 2 μs are more desirable, but of course, it will require a more powerful power modulator with a fast slew rate.

IV. Conclusion

The influence of the sample placement on the PIII dose uniformity on the groove surface of an industrial ball bearing is investigated using a two-dimensional fluid model. Our results indicate that direct placement of the bearing on the sample chuck is most undesirable and gives rise a very low ion implant dose near the groove upper edge due to glancing ion incidence. On the other hand, when the bearing is elevated from the sample stage using a metal extension, the ion dose uniformity along the groove surface is enhanced. The improvement is larger when using a thinner extension rod. However, due to insufficient heat dissipation via the sample stage, either the PIII duty cycle needs to be reduced or the extensive rod must be bigger for low temperature processes. However, a bigger extension rod draws more current and may require a more potent power supply and modulator. The ideal sample placement configuration depends on the processing requirements, especially the temperature window.

References

[1] J. R. Conrad, J. L. Radtke, R. A. Dodd, F. J. Worzala, and N. C. Tran, "Plasma source ion implantation technique for surface modification of materials," *J. Appl. Phys.*, vol. 62, no. 11, pp. 4591–4596, 1987.

[2] G. A. Collins, R. Hutchings, J. Tendys, and M. Samandi, "Advanced surface treatments by plasma ion implantation," *Surf. Coat. Technol.*, vols. 68/69, pp. 285–293, 1994.

[3] J. R. Conrad, R. A. Dodd, S. Han, M. Madapura, J. Scheuer, K. Sridharan, and F. J. Worzala, "Ion beam assisted coating and surface modification with plasma source ion implantation," *J. Vac. Sci. Technol. A*, vol. 8, no. 4, pp. 3146–3151, 1990.

[4] S. Y. Wang, P. K. Chu, B. Y. Tang, X. C. Zeng, Y. B. Chen, and X. F. Wang, "Radio-frequency plasma nitriding and nitrogen plasma immersion ion implantation of Ti_6Al_4V alloy," *Surf. Coat. Technol.*, vol. 93, nos. 2–3, pp. 309–313, 1997.

[5] S. Y. Wang, P. K. Chu, B. Y. Tang, X. C. Zeng, and X. F. Wang, "Improvement of the corrosion property of Cr_4Mo_4V bearing steel using plasma immersion ion implantation," *Nucl. Instrum. Methods B*, vols. 127/128, pp. 1000–1003, 1997.

[6] X. C. Zeng, B. Y. Tang, and P. K. Chu, "Improving the plasma immersion ion implantation impact energy inside a cylindrical bore by using an auxiliary electrode," *Appl. Phys. Lett.*, vol. 69, no. 25, pp. 3815–3817, 1996.

[7] X. C. Zeng, T. K. Kwok, A. G. Liu, P. K. Chu, B. Y. Tang, and T. E. Sheridan, "Effects of the auxiliary electrode radius during plasma immersion ion implantation of a small cylindrical bore," *Appl. Phys. Lett.*, vol. 71, no. 8, pp. 1035–1037, 1997.

[8] T. E. Sheridan, T. K. Kwok, and P. K. Chu, "Kinetic model for plasma-based ion implantation of a short, cylindrical tube with auxiliary electrode," *Appl. Phys. Lett.*, vol. 72, no. 15, pp. 1826–1828, 1998.

[9] X. C. Zeng, T. K. Kwok, A. G. Liu, P. K. Chu, and B. Y. Tang, "Plasma immersion ion implantation of the interior surface of a large cylindrical bore using an auxiliary electrode," *J. Appl. Phys.*, vol. 83, no. 1, pp. 44–49, 1998.
[10] T. E. Sheridan and M. J. Alport, "Two-dimensional model of ion dynamics during plasma source ion implantation," *Appl. Phys. Lett.*, vol. 64, no. 14, pp. 1783–1785, 1994.
[11] M. Hong and G. A. Emmert, "Two-dimensional fluid modeling of time-dependent plasma sheaths," *J. Vac. Sci. Technol. B*, vol. 12, no. 2, p. 889, 1994.
[12] S. M. Malik, D. E. Muller, K. Sridharan, R. P. Fetherston, and N. Tran, "Distribution of incident ions and retained dose analysis for a wedge-shaped target in plasma source ion implantation," *J. Appl. Phys.*, vol. 77, no. 3, pp. 1015–1019, 1995.
[13] W. Ensinger, T. Hochauer, and B. Rauschenbach, "Treatment uniformity of plasma immersion ion implantation studied with three-dimensional model systems," *Surf. Coat. Technol.*, vols. 103–104, pp. 218–221, 1998.
[14] P. A. Watterson, "Child-Langmuir sheath structure around wedge-shaped cathods," *J. Phys. D, Appl. Phys.*, vol. 22, pp. 1300–1307, 1989.
[15] T. E. Sheridan, "Sheath expansion at a corner," *J. Phys. D, Appl. Phys.*, vol. 29, pp. 2725–2728, 1996.
[16] T. E. Sheridan, "Pulsed sheath ion dynamics in a trench," *J. Phys. D, Appl. Phys.*, vol. 28, pp. 1094–1098, 1995.
[17] G. Keller, M. Paulus, S. Mandl, B. Stritzker, and B. Rauschenbach, "Modeling on plasma immersion implantation of trenches," *Nucl. Instrum. Methods B*, vol. 148, pp. 64–68, 1999.
[18] M. Hong and G. A. Emmert, "Two-dimensional fluid simulation of expanding plasma sheaths," *J. Appl. Phys.*, vol. 78, no. 12, pp. 6967–6973, 1995.
[19] S. Mandl, N. P. Barradas, J. Brutscher, R. Gunzel, and W. Moller, "Comparison of measured and calculated dose for plasma source ion implantation into 3-D objects," *Nucl. Instrum. Methods B*, vols. 127/128, pp. 996–999, 1997.
[20] S. Mandl, H. Reuther, J. Brutscher, R. Gunzel, and W. Moller, "Measured and calculated dose distribution for 2D plasma immersion ion implantation," *Surf. Coat. Technol.*, vol. 93, pp. 229–233, 1997.
[21] P. K. Chu, B. Y. Tang, Y. C. Cheng, and P. K. Ko, "Principles and characteristics of a new generation plasma immersion ion implanter," *Rev. Sci. Instrum.*, vol. 68, no. 4, pp. 1866–1874, 1997.
[22] M. Widner, I. Alexeff, and W. D. Jones, "Ion acoustic wave excitation and ion sheath evolution," *Phys. Fluids*, vol. 13, no. 10, pp. 2532–2537, 1970.

Zhaoming Zeng, for a photograph and biography, see p. 790 of the June 1999 issue of this TRANSACTIONS.

Xiubo Tian was born in 1969. He received the B.S. and M.S. degrees in materials science and technology from Harbin Institute of Technology (HIT), China, in 1990 and 1993, respectively. He is currently pursuing the Ph.D. degree at HIT and the City University of Hong Kong.

He joined the Plasma Laboratory of the City University of Hong Kong in July 1998 as a Research Assistant. His research interests are low energy, high frequency plasma immersion ion implantation, plasma and nitriding equipment and applications, and in-situ monitoring in plasma immersion ion implantation.

Dixon Tat-Kun Kwok (M'98), for a photograph and biography, see p. 237 of the February 1999 issue of this TRANSACTIONS.

Baoyin Tang, for a photograph and biography, see p. 789 of the June 1999 issue of this TRANSACTIONS.

Paul K. Chu (M'97), for a photograph and biography, see p. 238 of the February 1999 issue of this TRANSACTIONS.